ADVANCED MATERIALS

Supporting Information

for *Adv. Mater.*, DOI 10.1002/adma.202407070

Engineering d-p Orbital Hybridization with P, S Co-Coordination Asymmetric Configuration of Single Atoms Toward High-Rate and Long-Cycling Lithium–Sulfur Battery

Chenxu Dong, Changning Ma, Cheng Zhou, Yongkun Yu, Jiajing Wang, Kesong Yu, Chunli Shen, Jiapei Gu, Kaijian Yan, Aqian Zheng, Minjian Gong, Xu Xu and Liqiang Mai**

Engineering d-p orbital hybridization with P, S co-coordination asymmetric configuration of single atoms towards high-rate and long-cycling lithium-sulfur battery

Chenxu Dong, Changning Ma, Cheng Zhou, Yongkun Yu, Jiajing Wang, Kesong Yu, Chunli Shen, Jiapei Gu, Kaijian Yan, Aqian Zheng, Minjian Gong, Xu Xu*, Liqiang Mai*

State Key Laboratory of Advanced Technology for Materials Synthesis and Processing

International School of Materials Science and Engineering

Wuhan University of Technology, Wuhan 430070, Hubei, P. R. China

E-mails: xuxu@whut.edu.cn; mlq518@whut.edu.cn

Supporting Information

Experimental Section

In this study, all chemicals were used without further purification. Zinc nitrate hexahydrate (98%), cobalt nitrate hexahydrate ($Co(NO_3)_2·6H_2O$, 99.99%), bis(4-hydroxyphenyl) sulfone (98%) and phosphonitrilic chloride trimer (98%) were obtained from Macklin Chemistry Reagent Co. Ltd. Methanol, ethanol and N,N-diethylethanamine were obtained from Aladdin Chemistry Reagent Co. Ltd. $LiNO_3$ (99.9%), Li_2S, and sublimed sulfur powder were purchased from Alfa Aesar. In addition, 1,3-dioxlane (DOL) (99.5%) and 1,2-dimethoxyethane (DME) (99.5%) were used in this study.

Preparation of ZIF-8 and Co-ZIF-8.

3 mmol Zn $(NO_3)_2·6H_2O$ and 12 mmol 2-methylimidazole were dissolved in 50 ml of methanol, respectively, and stirred for 15 minutes. Then the above two solutions were mixed and vigorously stirred for 3 minutes at room temperature. Subsequently, the solution was maintained at 35 ℃ for 6 hours, and white precipitates appear at the bottom of the beaker. The synthesized white precipitate was centrifuged, washed and separated using methanol as a solvent. Then the product was dried at 80 ℃ to obtain white powder ZIF-8. The synthesis of Co-ZIF-8 followed the same steps, except for adding 0.05 mmol of cobalt nitrate.

Preparation of CoSA-N_3PS hollow nanocages.

The synthesized ZIF-8 powder (200 mg) was uniformly dispersed in 40 ml methanol. Then, 100 mL methanol solution containing bis (4-hydroxyphenyl) sulfone (160 mg) and phosphonitrile chloride trimer (75 mg) was added to the dispersion of ZIF-8 and was stirred for 15 minutes. Subsequently, 1 mL N, N-diethylethylethylamine was added slowly to the above dispersion system, and then stir at room temperature for 15 hours. The product was washed by methanol centrifugation and dried at 80 ℃ for 15 hours to obtain ZIF-8@PZS white powder. Add the above ZIF-8@PZS The powder was placed in a quartz boat and heated at a rate of 5 °C min^{-1} for 650 °C for 2 hours in a tube furnace under a flowing Ar atmosphere to obtain a hollow polyhedral structure. Then 200 mg powder was evenly dispersed in 50 mL methanol and treated with ultrasound. Next, 10 mg/mL of $Co(NO_3)_2 \cdot 6H_2O$ methanol solution was slowly added to the above dispersion system and stirred at room temperature for 24 hours, then the precipitate was washed, dry and collected. Finally, the above precipitate was placed in a quartz boat and heated up at a rate of 5 °C min^{-1} in a tube furnace under a flowing argon atmosphere at 950 °C for 3 hours. The final product is labeled as CoSA-N_3PS.

Preparation of CoSA-N_4 and NPS hollow nanocages.

The control sample of CoSA-N_4 was prepared using the same procedures, except for using Co-ZIF-8 as the precursor and removing the step of adding $Co(NO_3)_2 \cdot 6H_2O$ solution. The synthesis of NPS samples was carried out through one-step pyrolysis of ZIF-8@PZS at 800 °C.

Preparation of S@CoSA-N_3PS, S@CoSA-N_4, and S@NPS composites.

S@CoSA-N_3PS, S@CoSA-N_4, and S@NPS cathodes were prepared by a straightforward fusion-diffusion method. The host materials and sulfur were mixed in a ratio of 1:3, then ground using a mortar for 30 minutes, and heated at 155 °C for 12 hours in a glass container under an Ar atmosphere.

Li_2S_6 visualized adsorption tests

Li_2S and sulfur were mixed in 1,2-dimethoxyethane (DME) solution. The mixture was stirred at 70°C for 2 days to obtain a Li_2S_6 solution with a concentration of 2 mmol/L. Subsequently, 10 mg of CoSA-N_3PS, CoSA-N_4, and NPS were added to 3 mL Li_2S_6 solution, respectively. The resulting mixture was allowed to stand undisturbed for 6 hours.

The nucleation of Li_2S tests

A 0.25 mol L^{-1} Li_2S_8 solution was prepared by dissolving 57.5 mg Li_2S and 280 mg S_8 in 5 ml tetraglyme solution and stirring the mixture at 70℃ for 2 days. The cathode was prepared by pasting a slurry containing 80 wt% active material (CoSA-N_3PS, CoSA-N_4, or NPS), Super P (10 wt%), and PVDF (10 wt%) onto an aluminum foil collector plate. Lithium foil was used as the anode, and Celgard 2500 membrane was served as the separator. The coin cells were assembled by adding 10 μl Li_2S_8 catholyte onto the host materials and 10 μl blank electrolyte on the anode side. The cells were then

galvanostatically discharged to 2.06 V at a current of 0.112 mA and held at 2.05 V to initiate Li_2S nucleation until the current decreased to less than 10^{-5} A. To decompose Li_2S, the assembled cells were galvanostatically discharged to 1.70 V at 0.112 mA and then potentiostatically charged at 2.35 V until the charge current fell below 10^{-5} A.

Materials Characterizations.

Morphological information was obtained by scanning electron microscopy (SEM) using a JEOL JSM-7100F scanning electron microscope at a voltage of 10 kV. Aberration-corrected high-angle annular dark field scanning transmission electron microscopy (HAADF-STEM), transmission electron microscopy (TEM), and high-resolution transmission electron microscopy (HRTEM) images were acquired using a Titan G2 60-300 with an energy-dispersive X-ray (EDX) spectrometer. X-ray diffraction (XRD) was performed using a D8 Advance X-ray diffractometer with a non-monochromated Cu Kα X-ray source (λ = 1.054056 Å) to determine the crystallographic properties of the samples. The N2 adsorption/desorption isothermal was performed by the TriStar-3020 gas adsorption analyzer at 77 K (Micromeritics Instrument Co., USA). X-ray photoelectron spectroscopy (XPS) was performed using a VG MultiLab 2000 instrument.

Electrochemistry measurement.

Coin cells (2025-type) were assembled within an argon-filled glovebox. The cathode involved applying a slurry composed of 80 wt% active material (S@CoSA-N_3PS, S@CoSA-N_4, or S@NPS), Super P (10 wt%), and PVDF (10 wt%) on a carbon-coated aluminum foil collector plate. Subsequently, the resulting mixture underwent drying at 60°C and was then cut into circular pellets for assembling the batteries. The pellets were utilized directly as the cathode, while lithium foil was utilized as the anode. The electrolyte was a mixed solution of 1 M LiTFSI in DME and DOL with a volume ratio of 1:1, with $LiNO_3$ (1 wt%) added as an additive. The ratio of electrolyte to S (E/S) of coin cells was 15 (μL):1 (mg) and the ratio of E/S of pouch cell was 8 (μL):1 (mg). Cycling tests were conducted at a low current density during the initial few cycles. The galvanostatic charge/discharge cycling was conducted using the Neware battery test system (CT-4008-5V6A-S1-F, Shenzhen, China) with a potential range of 1.7-2.8 V vs. Li/Li^+. The cyclic voltammetry (CV) curves were performed using an electrochemical workstation (AutolabPGSTAT302N).

Calculation methods

The first-principles calculations based on density functional theory (DFT) were implemented in the Vienna Ab Initio Simulation Package (VASP), using the frozen-core projector augmented-wave (PAW) method to describe the interaction between the atomic cores and the valence electron density. The exchange-correlation potential was approximated within the generalized gradient approximation (GGA) using the Perdew-Burke Ernzerhof (PBE) functional. The dispersion corrected DFT-D3 schemes was employed to describe the Van der Waals (vdW) interactions. Plane-wave cutoff energy

was set to 500 eV. The conjugate gradient algorithm was used in ionic optimization, convergence threshold was set to 10^{-5} eV in electronic relaxation and 0.05 eV $Å^{-1}$ in Hellmann-Feynman force on each atom. The Brillouin zone in reciprocal space was sampled by a Γ-centered Monkhorst–Pack scheme with 2 × 2 × 1 k-point grids for geometry optimization of 6 × 6 × 1 supercell. The climbing image nudged elastic (CI-NEB) method was used to calculate the diffusion barriers of Li atom.

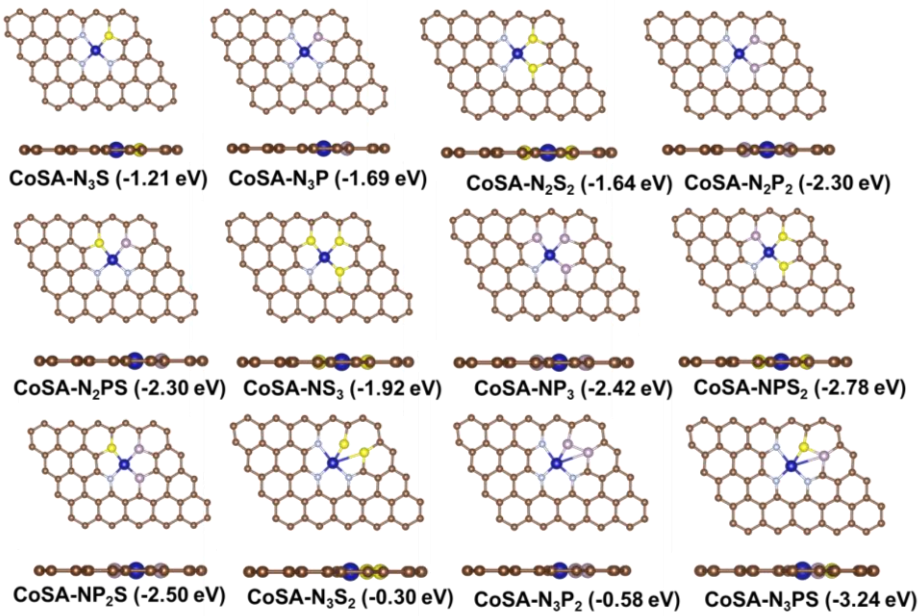

Figure S1. The model structures of CoSA-N_4, CoSA-N_3S, CoSA-N_3P, CoSA-N_2S_2, CoSA-N_2P_2, CoSA-N_2PS, CoSA-NS_3, CoSA-NP_3, CoSA-NPS_2, CoSA-NP_2S, CoSA-N_3P_2, CoSA-N_3S_2, CoSA-N_3PS and the corresponding total energies.

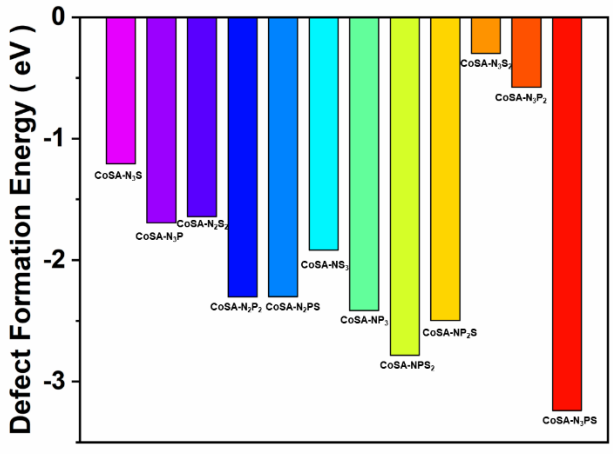

Figure S2. Comparison of total energy of different configurations.

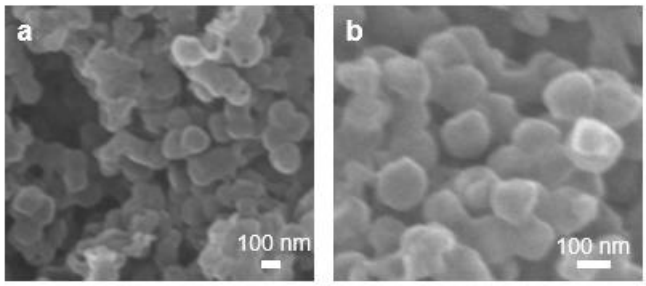

Figure S3. The SEM images of CoSA-N_3PS nanocages.

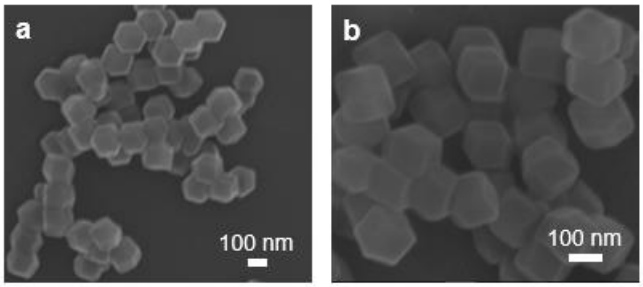

Figure S4. The SEM images of ZIF-8 nanoparticles.

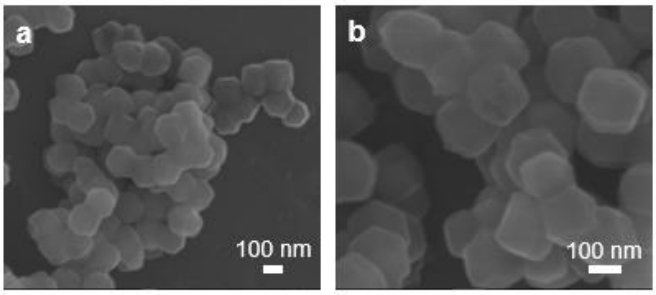

Figure S5. The SEM images of ZIF-8@PZS nanoparticles.

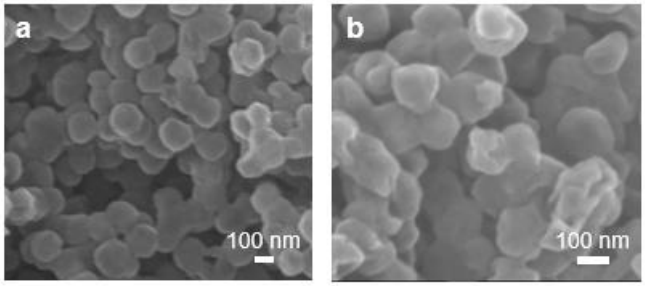

Figure S6. The SEM images of NPS nanocages.

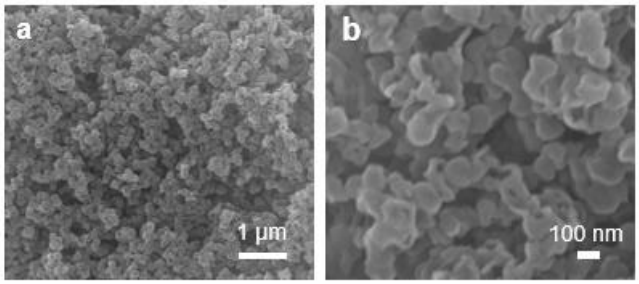

Figure S7. The SEM images of S@CoSA-N_3PS.

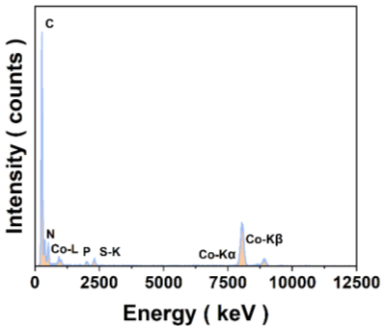

Figure S8. The EDS mapping of CoSA-N_3PS.

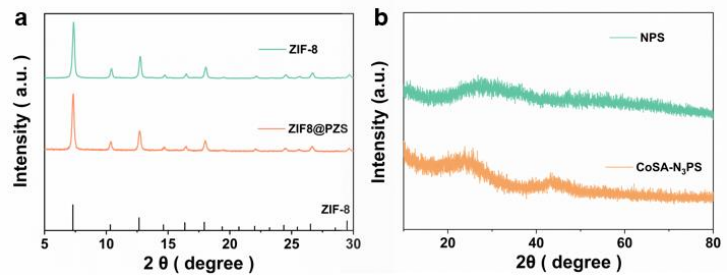

Figure S9. XRD patterns of ZIF-8, ZIF-8@PZS, NPS and CoSA-N_3PS.

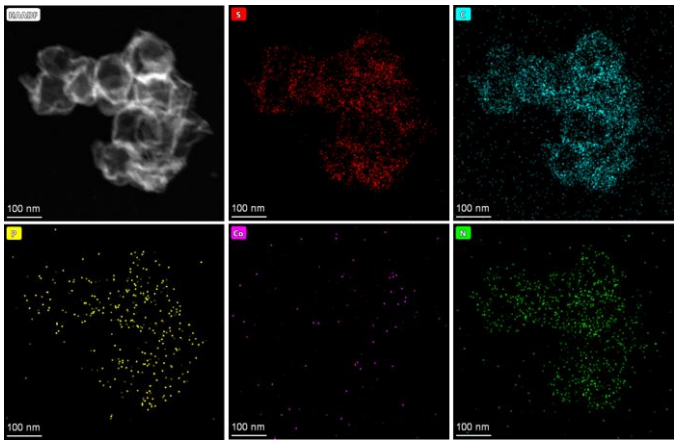

Figure S10. The the HADDF-STEM image and its corresponding EDS mappings of S@CoSA-N_3PS.

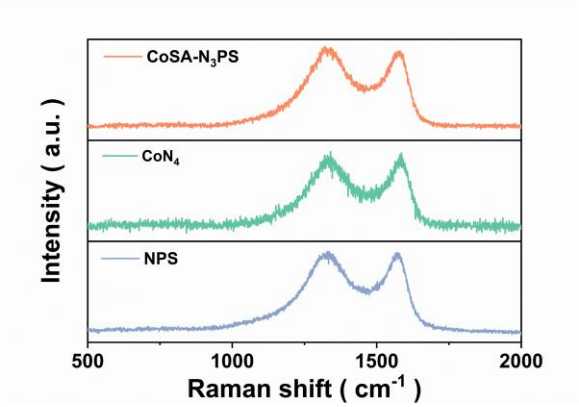

Figure S11. Raman spectra of the CoSA-N_3PS, CoSA-N_4, and NPS nanocages.

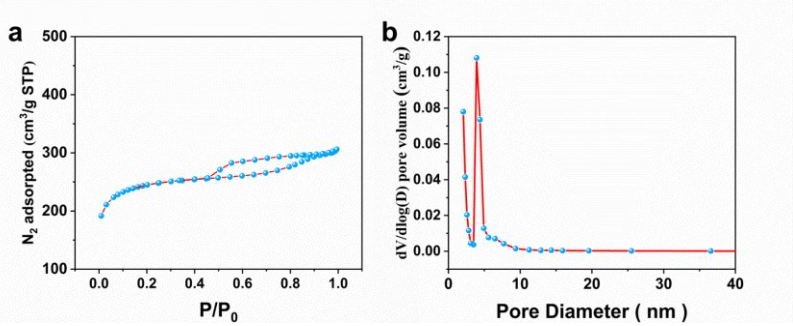

Figure S12. N_2 adsorption-desorption isotherms of the CoSA-N_3PS as well as its pore size distributions.

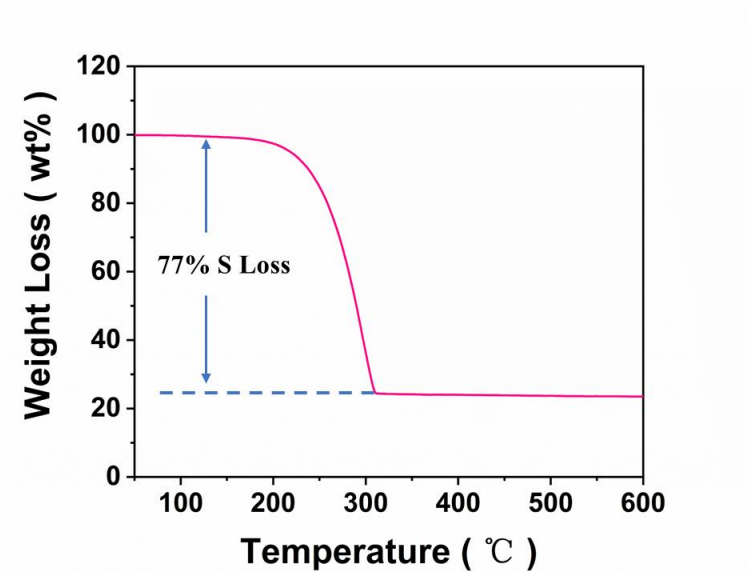

Figure S13. TGA curve of sulfur content with normal sulfur loading.

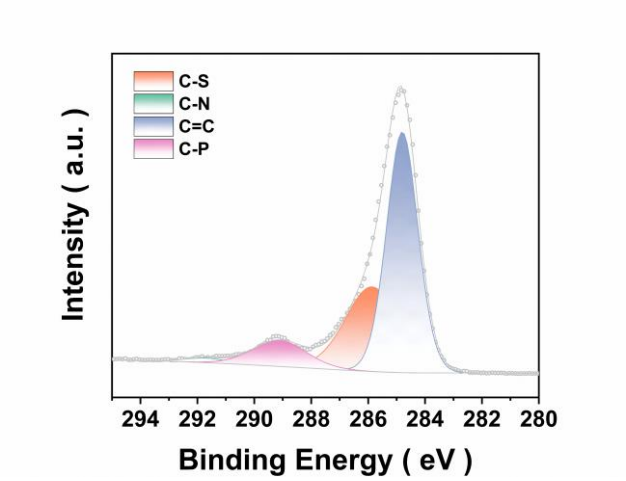

Figure S14. The XPS spectra of CoSA-N_3PS: C 1s spectra.

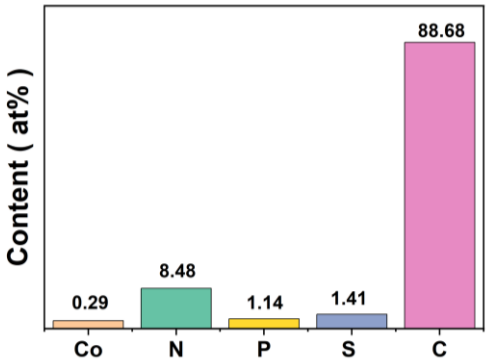

Figure S15. The element atomic content of Co, N, P, S and C in CoSA-N_3PS measured by XPS analysis.

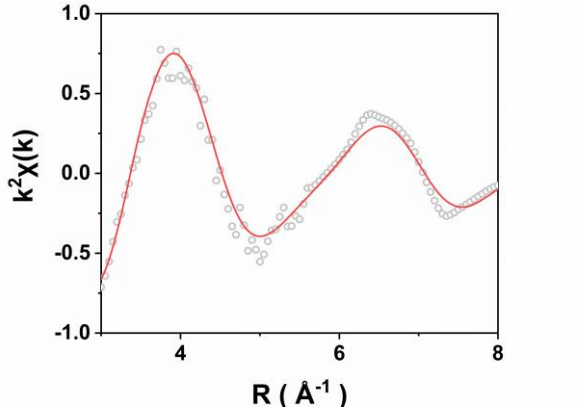

Figure S16. K-edge k-space experimental EXAFS spectra and fitting curves of Co.

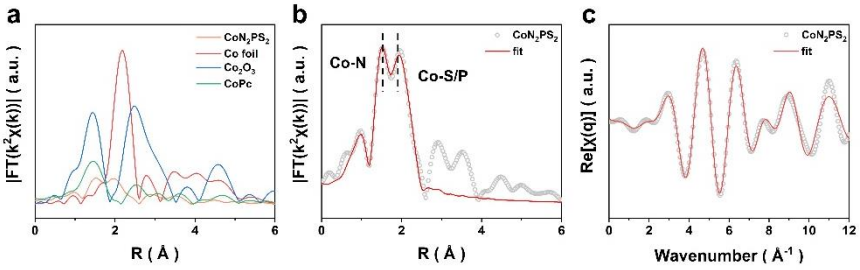

Figure S17. (a) FT-EXAFS at the Co K-edge. (b) FT-EXAFS fitting curves in the R space fitting curves of CoSA-N_2PS_2 (c) XANES spectra in q space and fitting curves of CoSA-N_2PS_2.

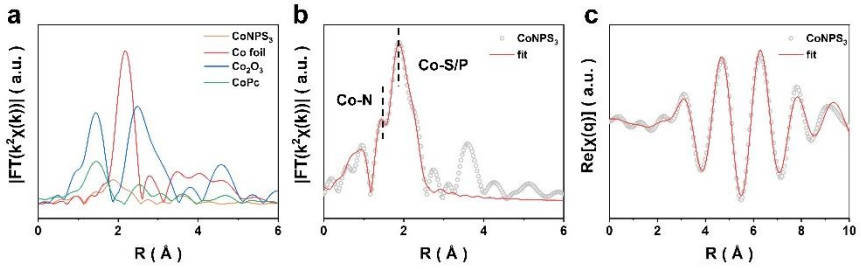

Figure S18. (a) FT-EXAFS at the Co K-edge. (b) FT-EXAFS fitting curves in the R space fitting curves of CoSA-NPS_3 (c) XANES spectra in q space and fitting curves of CoSA-NPS_3.

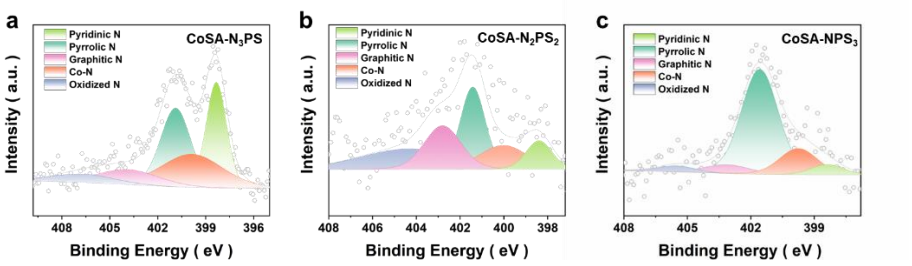

Figure S19. N 1s spectra of (a) CoSA-N_3PS, (b) CoSA-N_2PS_2 and (c) CoSA-NPS_3.

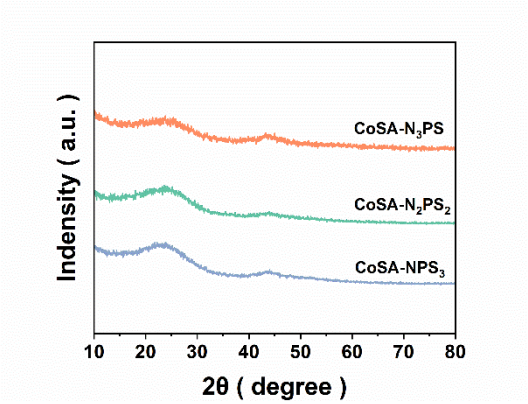

Figure S20. XRD patterns of CoSA-N_3PS, CoSA-N_2PS_2 and CoSA-NPS_3.

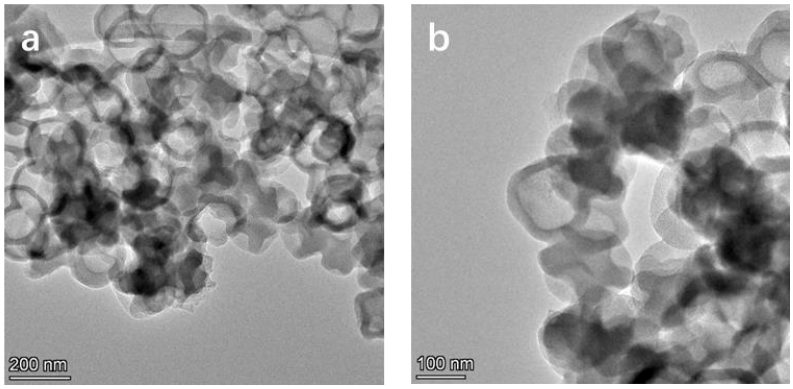

Figure S21. HRTEM images of CoSA-N_2PS_2.

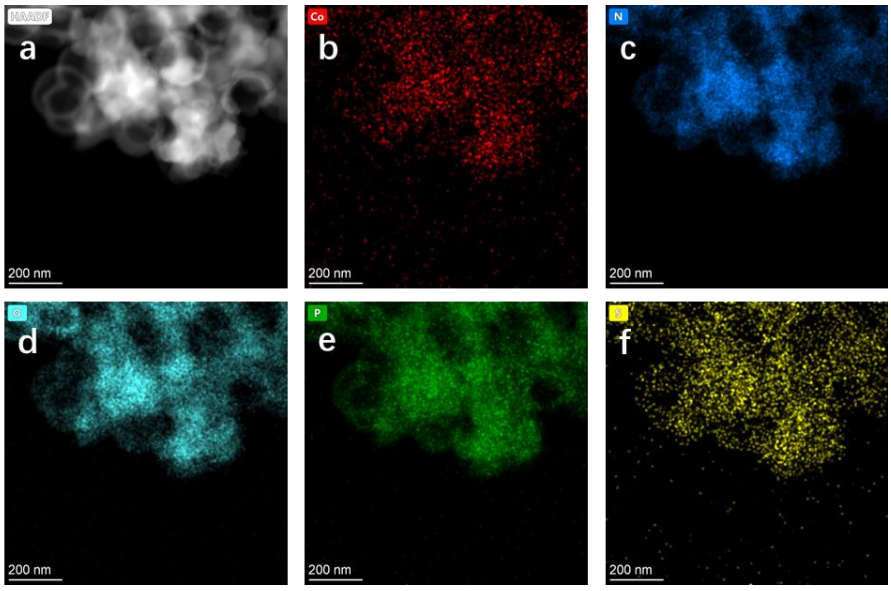

Figure S22. STEM image, and corresponding elemental mapping images of CoSA-N_2PS_2.

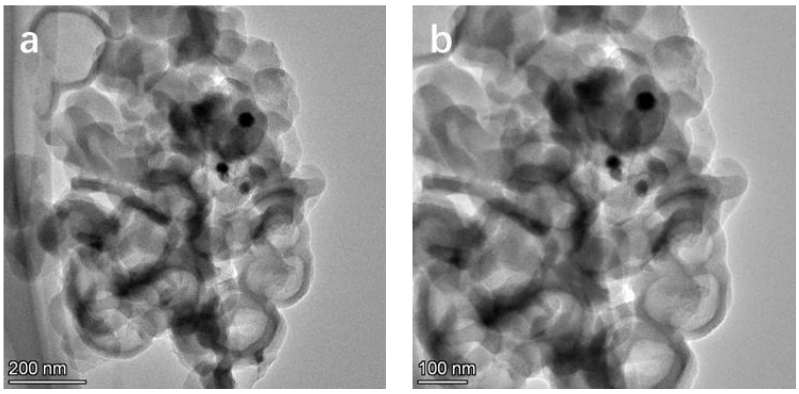

Figure 23. HRTEM images of CoSA-NPS_3.

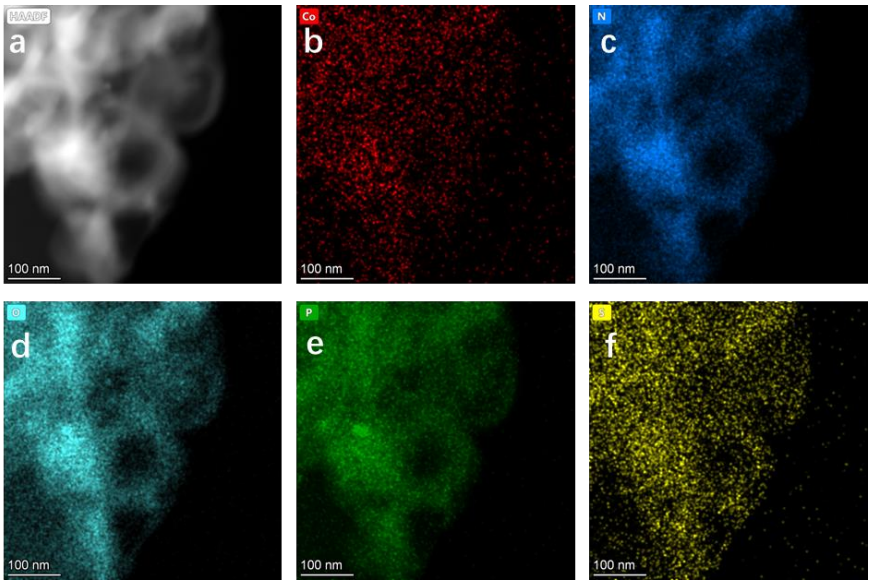

Figure 24. STEM image, and corresponding elemental mapping images of CoSA-NPS_3.

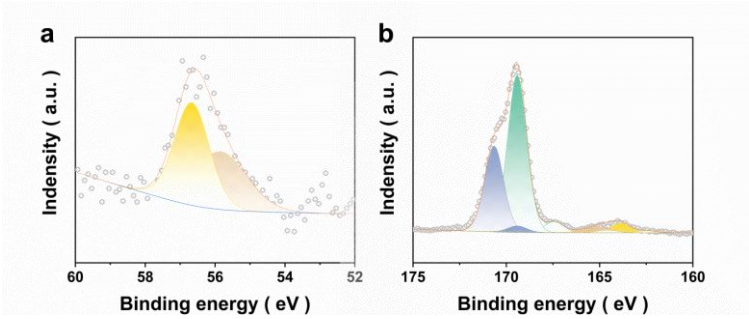

Figure S25. XPS spectra a) Li 1s spectrum and b) S 2p spectrum of CoSA-N_3PS/Li_2S_6 after 6 h.

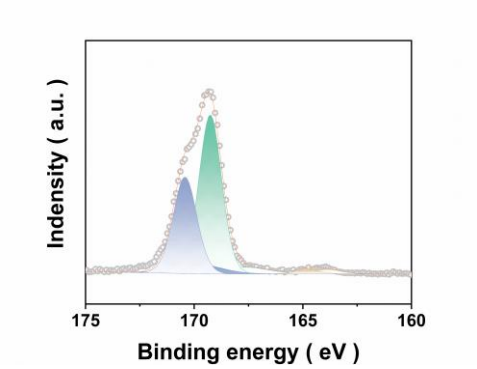

Figure S26. XPS spectra: S 2p spectrum of NPS/Li_2S_6 after 6 h.

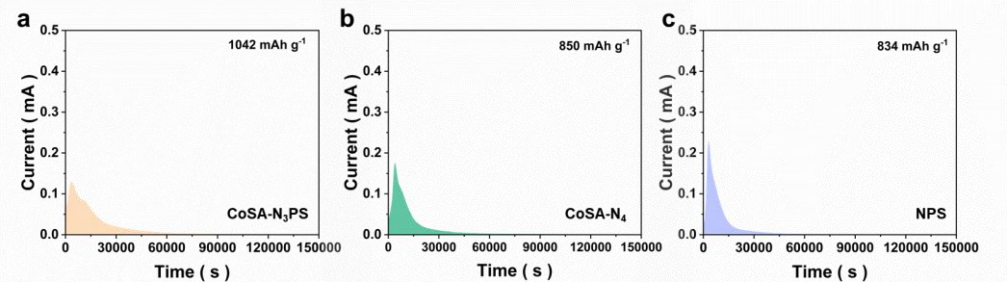

Figure S27. The dissolution profiles of Li_2S with CoSA-N_3PS, CoSA-N_4 and NPS electrodes.

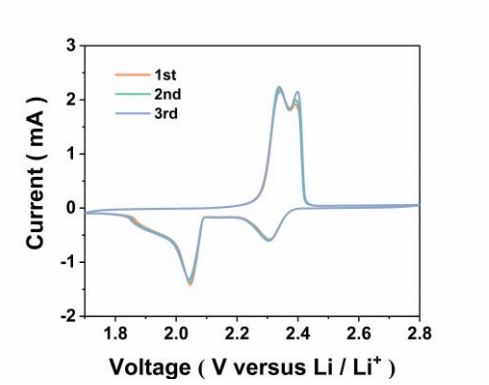

Figure S28. The initial three CV curves of S@CoSA-N_3PS cathode at 0.1 mV s^{-1}.

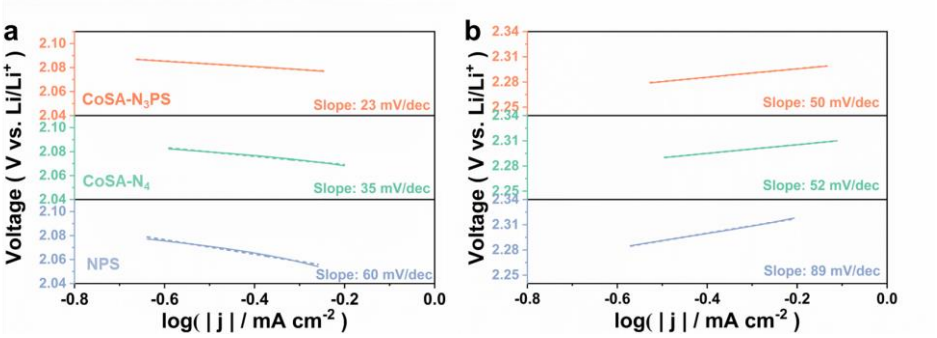

Figure S29. Tafel slopes from the cathodic peaks of the CV curves.

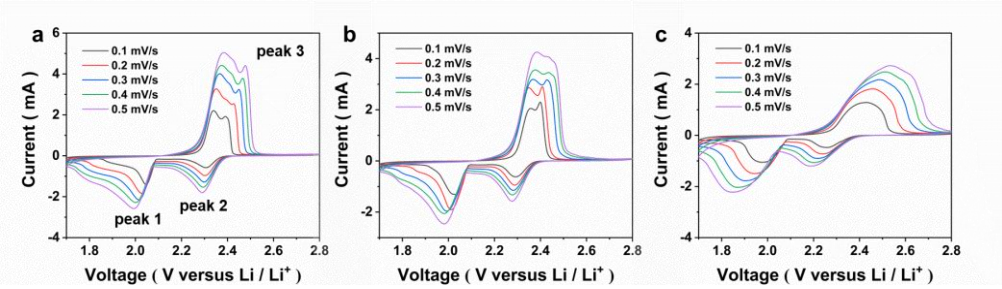

Figure S30. CV curves of S@CoSA-N_3PS, S@CoSA-N_4 and S@NPS cathodes at different scan rates in the range of 0.1-0.5 mV s^{-1}.

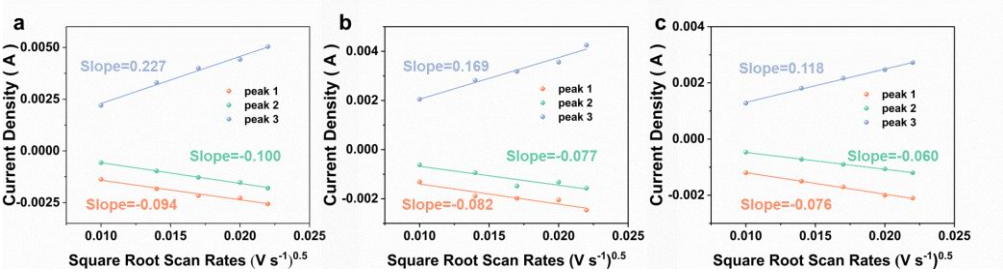

Figure S31. Currents for the peaks 1-3 shown in (e) as a function of the square root of the scan rate for S@CoSA-N_3PS, S@CoSA-N_4 and S@NPS cathodes.

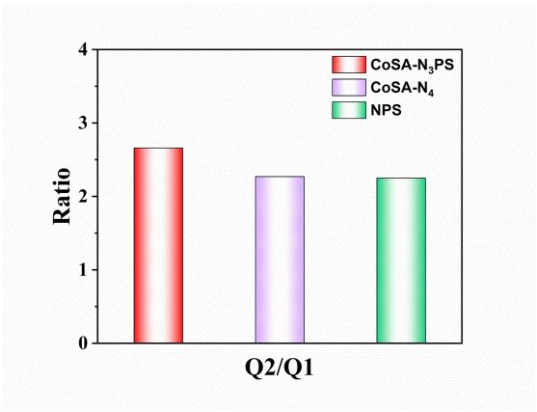

Figure S32. Values of Q2/Q1 obtained from charge/discharge curves.

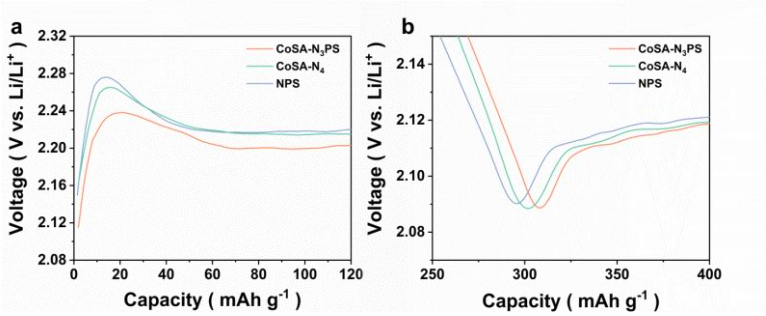

Figure S33. Charge and discharge curves of S@CoSA-N_3PS, S@CoSA-N_4 and S@NPS electrodes exhibiting the overpotentials for the conversion between soluble polysulfides and insoluble Li_2S_2/Li_2S.

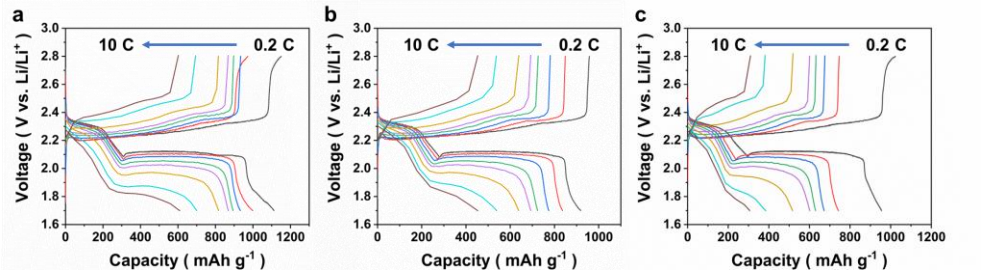

Figure S34. Galvanostatic charge-discharge profiles of the Li-S batteries with (a) S@CoSA-N_3PS cathode, (b) S@CoSA-N_4 cathode, and (c) S@NPS cathode at different rates in a potential window from 1.7 to 2.8V.

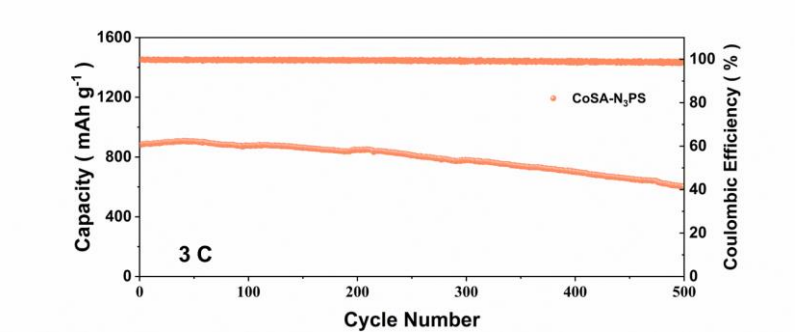

Figure S35. Long-term cycling performance at 3 C for 500 cycles.

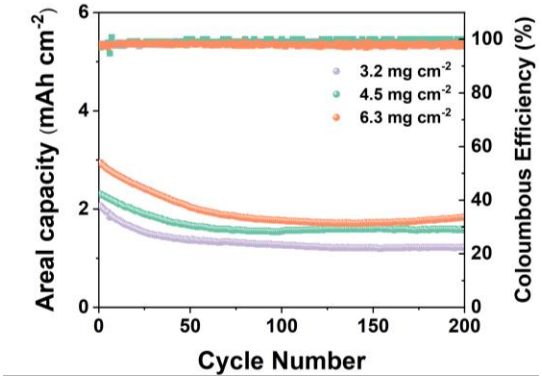

Figure S36. Cycling performances of S@CoSA-N_3PS cathodes with various sulfur loadings at 1 C.

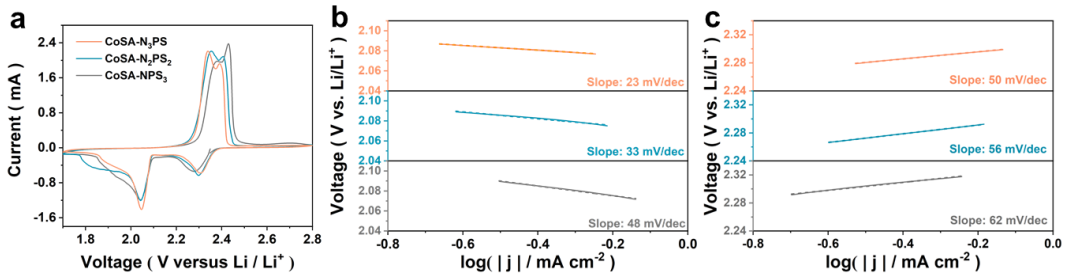

Figure S37. (a) CV curves of S@CoSA-N_3PS, S@CoSA-N_2PS_2, and S@CoSA-NPS_3 cathodes at 0.1 mV s^{-1} and (b-c) corresponding Tafel slopes from the CV curves.

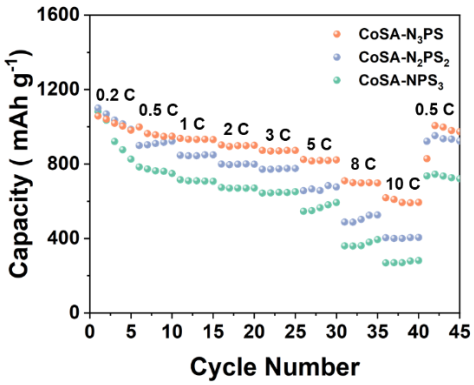

Figure S38. Rate performances of S@CoSA-N_3PS, S@CoSA-N_2PS_2, and S@CoSA-NPS_3 cathodes.

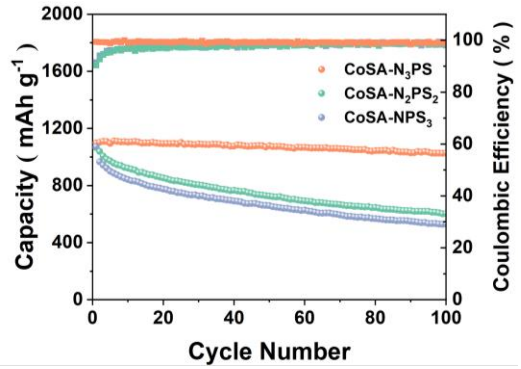

Figure S39. Cycling performances at 0.5 C of S@CoSA-N_3PS, S@CoSA-N_2PS_2, and S@CoSA-NPS_3 cathodes.

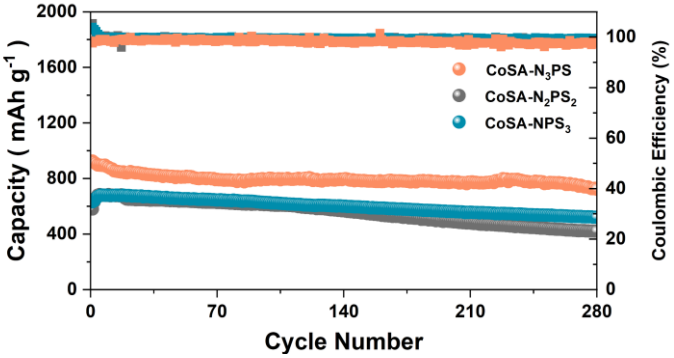

Figure S40. Cycling performances at 2 C of S@CoSA-N_3PS, S@CoSA-N_2PS_2, and S@CoSA-NPS_3 cathodes.

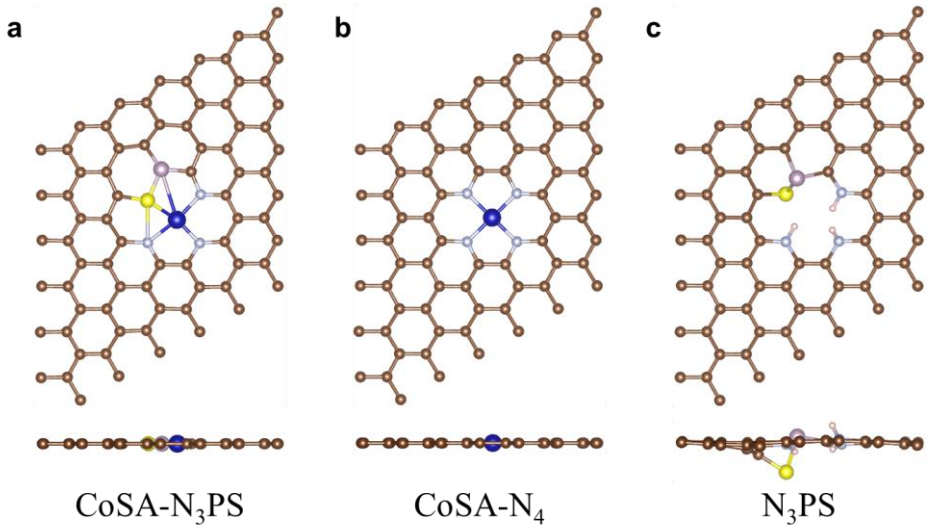

Figure S41. The optimized configurations of (a) CoSA-N_3PS, (b) CoSA-N_4, (c) NPS.

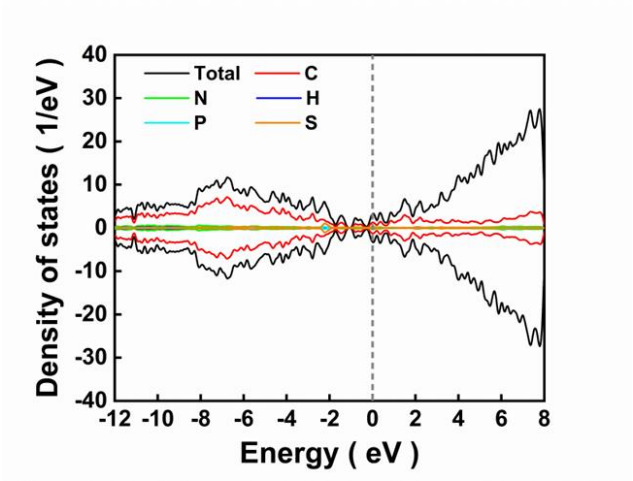

Figure S42. Density of states analysis of NPS.

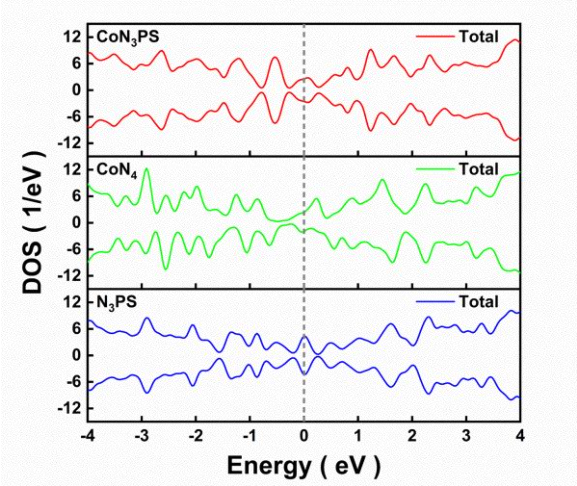

Figure S43. Total density of states analysis of different catalysts.

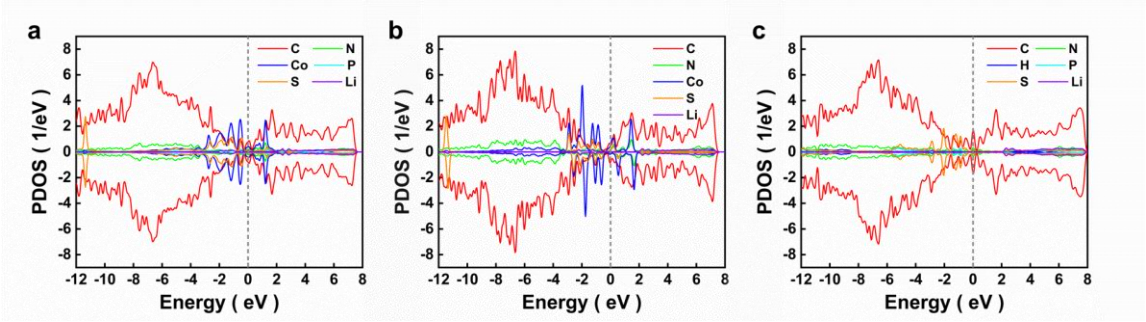

Figure S44. Density of states analysis of (a) CoSA-N_3PS, (b) CoSA-N_4, (c) NPS.

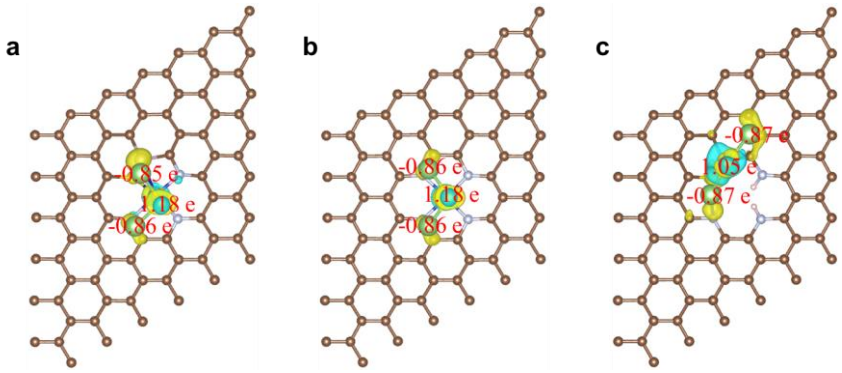

Figure S45. Simulated deformation charge density of (a) CoSA-N_3PS, (b) CoSA-N_4, (c) NPS.

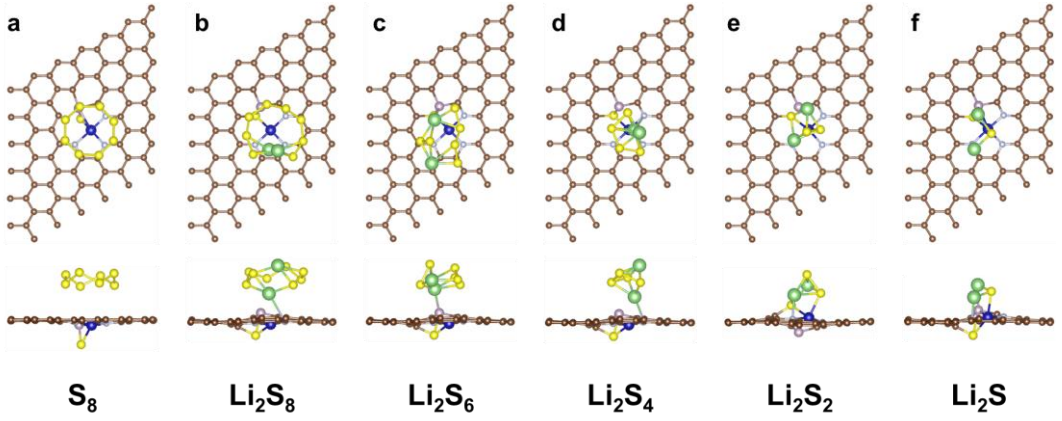

Figure S46. Optimized configurations of polysulfides on CoSA-N_3PS.

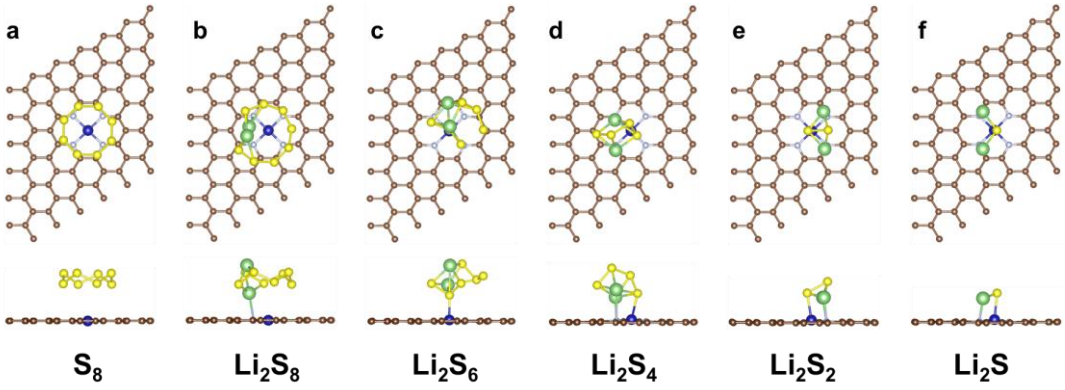

Figure S47. Optimized configurations of polysulfides on CoSA-N_4.

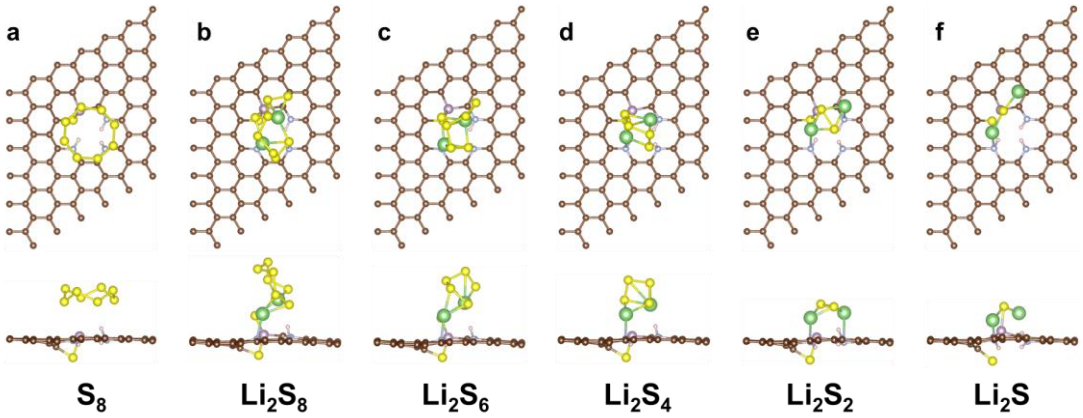

Figure S48. Optimized configurations of polysulfides on NPS.

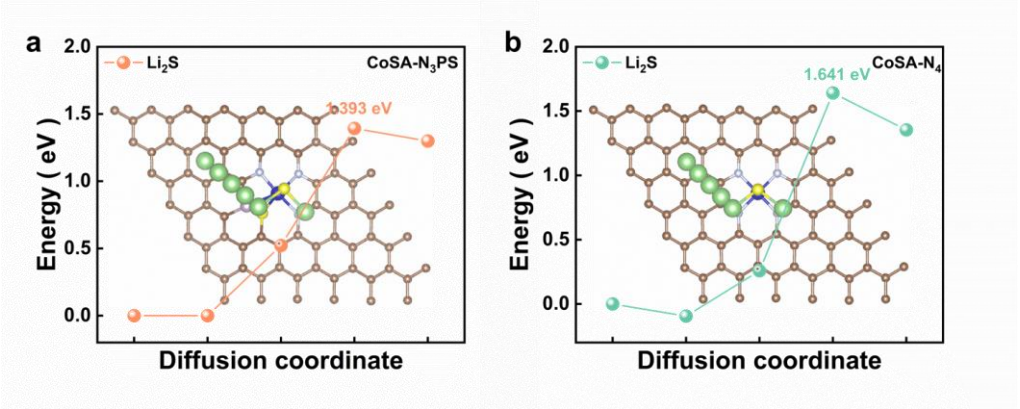

Figure S49. Decomposition energy barriers and corresponding decomposition pathways of Li_2S on CoSA-N_3PS and CoSA-N_4.

Table S1. The atomic ratios of Co, N, P, S, C elements in CoSA-N_3PS according to the EDS mapping.

Atomic ratio/%	C	N	P	S	Co
CoSA-N_3PS	88.38%	8.20%	1.32%	2.00%	0.10%

Table S2. The atomic ratios of Co, N, P, S, C elements in CoSA-N_3PS according to the ICP-OES and Elemental Analyzer.

Atomic ratio/%	N	P	S	Co
CoSA-N_3PS	9.31%	1.41%	2.07%	0.17%

Table S3. Structural parameters extracted from the Co K-edge EXAFS fitting.

Sample	Scattering Pair	CN	R (Å)	σ^2(Å^2)	ΔE0	R factor
CoSA-N_3PS	Co-N	3.2±0.4	1.87±0.02	0.0052±0.0031	2.3±0.4	0.008
	Co-P	1±0.2	2.31±0.01	0.0061±0.0023		
	Co-S	0.9±0.2	2.13±0.01	0.0059±0.0014		
CoSA-N_2PS_2	Co-N	2.2±0.3	1.86±0.04	0.0065±0.0022	3.5±1.3	0.01
	Co-P	0.9±0.2	2.34±0.07	0.0074±0.0025		
	Co-S	2.1±0.1	2.15±0.02	0.0083±0.0012		
CoSA-NPS_3	Co-N	1.1±0.2	1.81±0.03	0.0046±0.0014	3.2±0.6	0.009
	Co-P	0.9±0.2	2.37±0.05	0.0056±0.0020		
	Co-S	3.1±0.3	2.18±0.02	0.0057±0.0013		

Table S4. Comparison of the electrochemical performances of various single-atom catalysts reported in Li-S batteries.

Single atom	High sulfur loading (mg cm^{-2})	Rate capacity (mAh g^{-1})	Cycle performance			Ref.
			Initial capacity (mAh g^{-1})	Cycle number	Fading rate(%)	
CoSA-N_3PS	6	619 (10 C)	812 (5 C)	1000 2000 (1 C) (5 C)	0.04% 0.027%	This work
FeN_3P_1	6.4	659 (2 C)	700 (1 C)	800 (1 C)	0.04%	[1]
S-Co-SACs/NSC	7.8	722 (5 C)	881 (1 C)	500 (1 C)	0.05%	[2]
Fe/Co-N-HPC	4.8	740 (5 C)	977 (1 C)	300 (1 C)	0.10%	[3]
NC@SA-Co	4.1	582 (5 C)	750 (2 C)	700 (2 C)	0.06%	[4]
Ni-N_5/HNPC	5.1	684 (4 C)	1085 (0.5 C)	500 (0.5 C)	0.05%	[5]
Fe-N_5-C	8.2	723 (3 C)	906 (1 C)	500 (1 C)	0.05%	[6]
Co-NG	11.8	648 (6 C)	972 (0.5 C)	600 (0.5 C)	0.08%	[7]
Co-CMP	N/A	766 (2 C)	995 (0.5 C)	1000 (0.5 C)	0.05%	[8]
SAV@NG	N/A	645 (3 C)	780 (0.5 C)	400 (0.5 C)	0.07%	[9]
Co-N-C	11.3	1035 (2 C)	1161 (0.5 C)	300 (0.5 C)	0.10%	[10]
Ni@NG	N/A	612 (10 C)	1059 (1 C)	500 (1 C)	0.04%	[11]

Reference

[1] Huang, T.; Sun, Y.; Wu, J.; Shi, Z.; Ding, Y.; Wang, M.; Su, C.; Li, Y.; Sun, J. Altering Local Chemistry of Single-Atom Coordination Boosts Bidirectional Polysulfide Conversion of Li–S Batteries. *Adv. Funct. Mater.*, **2022**, 32, 2203902.

[2] Sun, T.; Huang, F.; Liu, J.; Yu, H.; Feng, X.; Feng, X.; Yang, Y.; Shu, H.; Zhang, F. Strengthened d-p Orbital-Hybridization of Single Atoms with Sulfur Species Induced Bidirectional Catalysis for Lithium–Sulfur Batteries. *Adv. Funct. Mater.*, **2023**, 2306049.

[3] Ma, L.; Qian, J.; Li, Y.; Cheng, Y.; Wang, S.; Wang, Z.; Peng, C.; Wu, K.; Xu, J.; Manke, I.; Yang, C.; Adelhelm, P.; Chen, R. Binary Metal Single Atom Electrocatalysts with Synergistic Catalytic Activity toward High-Rate and High Areal-Capacity Lithium-Sulfur Batteries. *Adv. Funct. Mater.*, **2022**, 32, 2208666.

[4] Li, Y.; Zhou, P.; Li, H.; Gao, T.; Zhou, L.; Zhang, Y.; Xiao, N.; Xia, Z.; Wang, L.; Zhang, Q.; Gu, L.; Guo, S. A Freestanding Flexible Single-Atom Cobalt-Based

Multifunctional Interlayer toward Reversible and Durable Lithium-Sulfur Batteries. *Small Methods*. **2020**, 4, 1900701.

[5] Zhang, S.; Ao, X.; Huang, J.; Wei, B.; Zhai, Y.; Zhai, D.; Deng, W.; Su, C.; Wang, D.; Li, Y. Isolated Single-Atom Ni–N $_5$ Catalytic Site in Hollow Porous Carbon Capsules for Efficient Lithium–Sulfur Batteries. *Nano Lett.,* **2021**, 21, 9691-9698.

[6] Zhang, Y.; Liu, J.; Wang, J.; Zhao, Y.; Luo, D.; Yu, A.; Wang, X.; Chen, Z. Engineering Oversaturated Fe-N $_5$ Multifunctional Catalytic Sites for Durable Lithium-Sulfur Batteries. *Angew. Chem. Int. Ed.,* **2021**, 60, 26622-26629.

[7] Meng, X.; Liu, X.; Fan, X.; Chen, X.; Chen, S.; Meng, Y.; Wang, M.; Zhou, J.; Hong, S.; Zheng, L.; Shi, G.; Bielawski, C. W.; Geng, J. Single-Atom Catalyst Aggregates: Size-Matching is Critical to Electrocatalytic Performance in Sulfur Cathodes. *Adv. Sci*., **2022**, 9, 2103773.

[8] Fan, X.; Chen, S.; Gong, W.; Meng, X.; Jia, Y.; Wang, Y.; Hong, S.; Zheng, L.; Zheng, L.; Bielawski, C. W.; Geng, J. A Conjugated Porous Polymer Complexed with a Single-Atom Cobalt Catalyst as An Electrocatalytic Sulfur Host for Enhancing Cathode Reaction Kinetics. *Energy Storage Mater*., **2021**, 41, 14-23.

[9] Zhou, G.; Zhao, S.; Wang, T.; Yang, S.-Z.; Johannessen, B.; Chen, H.; Liu, C.; Ye, Y.; Wu, Y.; Peng, Y.; Liu, C.; Jiang, S. P.; Zhang, Q.; Cui, Y. Theoretical Calculation Guided Design of Single-Atom Catalysts toward Fast Kinetic and Long-Life Li–S Batteries. *Nano Lett.,* **2020**, 20, 1252–1261.

[10] Li, B.; Kong, L.; Zhao, C.; Jin, Q.; Chen, X.; Peng, H.; Qin, J.; Chen, J.; Yuan, H.; Zhang, Q.; Huang, J. Expediting redox kinetics of sulfur species by atomic-scale electrocatalysts in lithium–sulfur batteries. *InfoMat*, **2019**, 1, 533-541.

[11] Zhang, L.; Liu, D.; Muhammad, Z.; Wan, F.; Xie, W.; Wang, Y.; Song, L.; Niu, Z.; Chen, J. Single Nickel Atoms on Nitrogen-Doped Graphene Enabling Enhanced Kinetics of Lithium-Sulfur Batteries. *Adv. Mater.,* **2019**, 31, 1903955.